AIAA Propulsion and Energy Forum
August 9-11, 2021, VIRTUAL EVENT
AIAA Propulsion and Energy 2021 Forum

10.2514/6.2021-3439

Monopropellant-Electrospray Multimode Thruster Testing Results: Electrospray Mode

Christopher T. Lyne[1] and Joshua L. Rovey[2]
University of Illinois at Urbana-Champaign, Urbana, IL, 61801, United States

Steven P. Berg[3]
Froberg Aerospace LLC., Wilmington, NC, 28401, United States

Multimode propulsion is the combination of two or more propulsive modes into a system that shares a single propellant, providing more flexibility than traditional propulsion systems. We report for the first time the electrospray operation of a multimode microthruster that can be switched between chemical monopropellant and capillary electrospray modes. We also demonstrated for the first time that the multimode propellant FAM-110A (59% wt. HAN, 41% wt. [Emim][$EtSO_4$], <1% H_2O), which was specifically designed for multimode monopropellant-electrospray propulsion, can be stably electrosprayed from a multi-emitter capillary thruster. Using a six-emitter subset of the thruster, stable electrospray operation is demonstrated for 10+ hours using the conventional ionic liquid propellant Emi-Im, and for 4+ hours using multimode propellant FAM-110A. Retarding potential analysis of the Emi-Im plume shows that the energy profile is nearly identical to that of similarly-sized single capillary emitters in the literature, implying that the thruster is operating in the mixed ion-droplet regime. The effects of hydraulic impedance on electrospray operating regime are briefly discussed. A simple analysis of capillary electrospray thrusters in the literature suggests that an emitter hydraulic impedance of $Z > 10^{16}$ Pa-s/m^3 is required to reach sufficiently low flow rates to suppress droplet emission.

I. Nomenclature

A	=	Cross-sectional area, [m^2]
I	=	Current, [A]
L	=	Length, [m]
P	=	Pressure, [Pa]
Q	=	Volumetric flow rate, [m^3/s]
R	=	Radius, [m]
Z	=	Hydraulic impedance, [Pa-s/m^3]
μ	=	Dynamic Viscosity, [Pa-s]
φ	=	Electric Potential, [V]

[1] Graduate Fellow, Department of Aerospace Engineering, AIAA Student Member.
[2] Associate Professor, Department of Aerospace Engineering, AIAA Associate Fellow.
[3] Chief Executive Officer, Froberg Aerospace LLC.

Emi-Im	=	1-ethyl-3-methylimidazolium bis(triflouromethylsulfonyl)amide; (a.k.a. Emi-Tf_2N)
Emim-$EtSO_4$	=	1-ethyl-3-methylimidazolium ethylsulfate
FAM-110A	=	Froberg Aerospace Multimode Propellant 110A (41%-59% wt. [Emim][$EtSO_4$]-HAN)
HAN	=	Hydroxylammonium nitrate
IL	=	Ionic liquid
MEPS	=	Monoprop-Electrospray Propulsion System
MMP	=	Multimode propulsion
RPA	=	Retarding potential analyzer

II. Introduction

The number of CubeSat (1 kg – 10 kg) launches have risen rapidly over the past decade, reaching more than 120 in 2015 [1]. Despite this growth, there are few propulsion options suitable for CubeSats and other NanoSats, perhaps due to the challenge of scaling down many mature propulsion technologies to meet the size and mass constraints [2]. Clearly, CubeSats would become significantly more capable if suitable low cost, versatile propulsion options are developed and made widely available. The wide variety of missions planned for CubeSats make obvious the need for propulsion system options that can reach a wide mission space, especially with regard to thrust and specific impulse. Effective propulsion solutions for CubeSats must be flexible and delivered at low cost.

Multimode propulsion (MMP) is a class of propulsion system that that shares propellant between two or more 'modes' of propulsion. The propellant is held in a single, shared tank, and can be allocated between the propulsive modes as needed. MMP systems typically combine a high-thrust mode with a high-specific impulse mode to cover a large mission space [3]. This approach is inherently flexible, and MMP systems can execute a far wider set of missions than traditional propulsion systems [3]. For example, the velocity change requirement of a mission can be met by the MMP system, and any excess fuel can be used to maximize the transfer rate. This characteristic makes MMP a good candidate for large-scale production, since a single MMP system can meet the requirements of a wide variety of missions. Furthermore, by sharing a single propellant tank, MMP can save mass and volume over a comparable approach using two fully separate propulsion systems [3], [4]. These advantages make MMP worth pursuing as a propulsion approach for small satellites.

A wide range of MMP concepts have been studied, most of which combine chemical and electric modes [4]. The principal challenge in developing chemical-electric MMP systems is finding a propellant that is suitable for both propulsion modes. Typically, electric propulsion devices use Xenon or other inert propellants, while chemical propellants are necessarily chemically reactive. MMP propellants have been surveyed, and some ionic liquids have emerged as candidates [4]–[6]. One MMP concept that uses ionic liquid propellants and is particularly suitable for miniaturization is combining monopropellant and electrospray propulsion. Froberg Aerospace LLC has developed a MMP microthruster on this concept, called the Monoprop-Electrospray Propulsion System (MEPS) microthruster, which combines chemical monopropellant and capillary electrospray modes into a MMP system that shares propellant and thruster hardware between modes. The microthruster consists of approximately 250 microchannels, each of which can act as a capillary electrospray emitter or a catalytic microchannel for monopropellant combustion.

The body of work leading to the development of the MEPS thruster is reviewed extensively by Rovey et al. [4]. Donius and Rovey assessed ionic liquids (ILs) as candidate propellants for combined monopropellant-electrospray MMP and found that IL propellants paired with hydroxylammonium nitrate (HAN) oxidizer have a comparable specific impulse to hydrazine [7]. Fonda-Marsland and Ryan also investigated ILs for chemical-electrospray propellants, and described the tradeoff between propellant properties required for each mode [8]. Berg and Rovey investigated imidazole-based ILs paired with HAN and reached a similar conclusion [6], [9]. Later, they synthesized propellant mixtures and evaluated their decomposition on a heated catalyst bed [10], [11]. Berg and Rovey's more recent work has focused on a 41%-59% wt. blend of Emim-$EtSO_4$ and HAN, also known as FAM-110A (Froberg Aerospace Multimode Propellant 110A). They demonstrated that platinum is an effective catalyst for FAM-110A [12], and showed that it can be decomposed in a heated platinum microtube [13]. Mundahl et al. evaluated the linear burn rates of potential chemical-electrospray IL propellants [12], [14], [15]. For FAM-110A, Mundahl et al. measured a linear burn rate of 22.8-26.5 mm/s at 1.5 MPa [12], [15] and Rasmont et al. measured a burn rate of 10-15 mm/s at 1

MPa [16]. In addition to evaluating chemical-mode performance, Berg and Rovey [5] and Wainwright et al. [17], [18] demonstrated stable electrospray of FAM-110A.

This paper describes the capillary electrospray mode operation and test results for the MEPS microthruster. We operate the microthruster with 6 microchannels (emitters) active using the ionic liquid propellant Emi-Im (Emi-Tf_2N) and the monopropellant-electrospray MMP propellant FAM-110A. For Emi-Im, retarding potential measurements show that the MEPS electrospray plume has similar energy properties to a single capillary electrospray source operating in the mixed ion-droplet regime. We also discuss the role of hydraulic impedance in determining the performance of capillary electrospray devices.

III. Experimental

A. MEPS Microthruster

The MEPS microthruster (Fig. 1), developed by Froberg Aerospace LLC, is designed to function as both a monopropellant thruster and a capillary electrospray thruster, and to be switchable between those modes. The thruster consists of a stainless steel block containing 256 microfluidic channels arranged in a 16 by 16 array, called the *microchannel array* or the *emitter array*. Each microchannel is lined with a catalyst layer, and each has a sharpened emitter tip at the microchannel exit. For monopropellant operation, the emitter array is heated and propellant is fed at a high rate. The propellant exothermically decomposes on contact with the catalyst, and the gaseous products are expelled from the microchannels to produce thrust. Recent tests of the thruster operating in chemical mode have demonstrated stable burn times up to 45 seconds [19]. For electrospray operation, a voltage difference is applied between the array block and the extractor electrode, and propellant is fed at a low rate through the channels. At the end of each microchannel, the propellant wets the emitter tip and forms a meniscus at the liquid-vacuum interface. With sufficient applied voltage, that meniscus deforms into a Taylor cone and begins producing a mixed beam of ions and charged droplets. The charged particles are accelerated by the applied voltage, then pass through the extractor aperture to leave the system. This momentum flux is responsible for the thrust produced by electrospray.

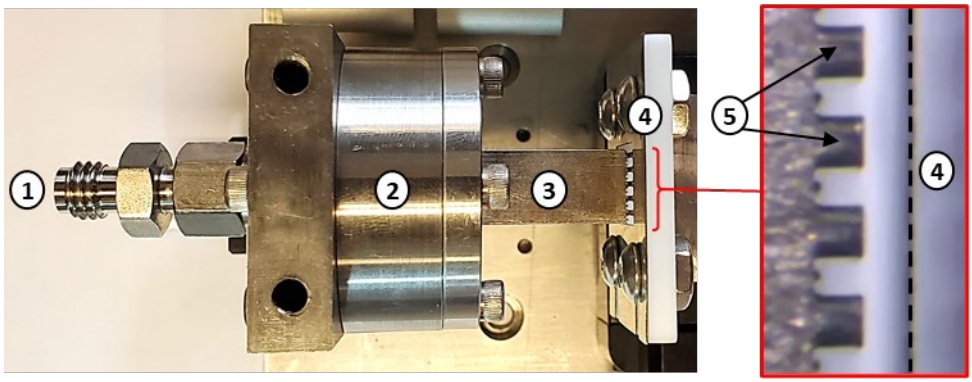

Figure 1: MEPS Thruster ready for an electrospray test. (1) Propellant inlet, (2) Propellant manifold, (3) Emitter array (a.k.a. microchannel array), (4) Extractor electrode, (5) Emitter tips.

Each microchannel is ~25 mm long, has an area-equivalent inner diameter of ~140 µm and an emitter tip outer diameter of ~350 µm. A ~200 µm thick, stainless steel extractor electrode with 1250 µm wide aperture slots is aligned with the emitter tips. A 500 µm vacuum gap separates the extractor from the emitter tips. This geometry results in an extractor acceptance angle of ~50°. In other words, we expect that plume species that are <50° off centerline will pass through the extractor aperture, while plume species that are >50° off centerline will impinge on the extractor. The extractor is mounted on a precision 5-axis stage and is aligned with the emitter tips using a microscope.

B. Monopropellant-Electrospray Compatible Propellant

The dual functionality of the MEPS thruster places unique requirements on the choice of propellant. It must be chemically reactive for monopropellant mode, but also be electrically conductive and have a low vapor pressure for electrospray mode. Ionic liquids (liquid salts) emerge as a viable candidate due to the wide variety of available ionic liquids and their generally low volatility and reasonable conductivity. Recent research has investigated the use of ionic liquids as propellants for chemical rockets [20], [21]. In particular, hydroxylamonium nitrate [HAN] has been suggested as a green alternative to hydrazine [22]–[24]. HAN is a principal component of several monopropellants but is typically in solution with water and is thus too volatile for electrospray applications. An ionic liquid mixture of

59% wt. HAN and 41% wt. 1-ethyl-3-methylimidazolium ethyl sulfate ([Emim][$EtSO_4$]) has been developed as a monopropellant-electrospray multimode propellant and is called FAM-110A (Froberg Aerospace Multimode Propellant 110A). This binary mixture has <1% water content, low toxicity, and has a theoretical specific impulse ~1% lower than hydrazine and a ~50% higher storage density [6], [14], [15]. FAM-110A has been successfully tested as catalytic monopropellant and electrospray propellant [5], [13], [15]–[17]. Its low volatility and low toxicity, high storage density, and high energetic content make FAM-110A an excellent candidate for monopropellant-electrospray multimode propulsion.

C. Feed System and Hydraulic Impedance

1. Feed System Overview

A schematic of the propellant feed system is shown in Figure 2. Propellant is held in a borosilicate propellant reservoir (1) that is attached to a dedicated vacuum pump and dry nitrogen supply. Metering valves are used to control the flow rate of nitrogen (3) and the conductance of the vacuum line (2), allowing control of the feed pressure from atmosphere down to ~150 mTorr. Feed (reservoir) pressure is measured using a vacuum gauge (6) (MKS 902B) with high accuracy in the relevant pressure range (>50 Torr). A clear polymer tube (Fluorinated ethylene propylene, 250µm I.D., 1/16" O.D., 1.52 m long) dips below the liquid level in the propellant reservoir and runs to the thruster inlet (7) via chamber feedthroughs. The same system can be used to degas propellant in order to remove volatiles before an electrospray test. For degassing, the reservoir is isolated from the N_2 supply and rough vacuum via (4) and the chamber-reservoir isolation valve (5) is opened, exposing the propellant reservoir to high vacuum (~10^{-5} Torr).

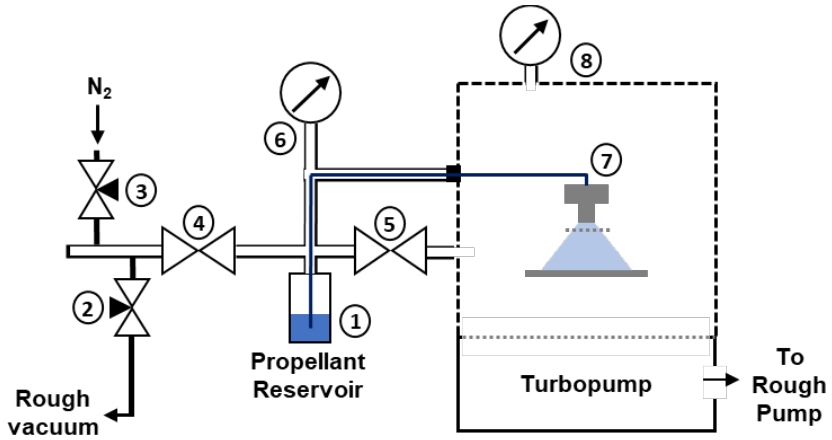

Figure 2: Propellant feed system diagram. (1) Propellant vial/reservoir, (2) Rough vacuum metering valve, (3) N_2 supply metering valve, (4) High vacuum isolation valve, (5) Chamber-reservoir isolation valve, (6) Feed pressure gauge, (7) Thruster, (8) Vacuum chamber and chamber vacuum gauge.

2. Flow Rate Estimation and Hydraulic Impedance

Flow through the feed tube is laminar with Re << 1, thus the flow rate can be modeled using the Hagen-Poiseuille equation for laminar flow in pipes of constant circular cross section (Equation 1).

$$\Delta P = \frac{8\mu L Q}{\pi R^4} = \frac{8\pi\mu L Q}{A^2} \qquad \text{Eq. 1}$$

An important feature of Hagen-Poiseuille flow is that the flow rate scales linearly with pressure drop. This property makes it possible to define a hydraulic impedance [25] that is analogous to electrical impedance in Ohm's law. That is, we seek to define hydraulic impedance Z such that Z = △P/Q. Rearranging Equation 1 and applying this definition of hydraulic impedance, we find that the hydraulic impedance for laminar flow through a pipe of constant circular cross section is given by Equation 2. We can extend this analogy to noncircular cross sections as well, though not rigorously because the Hagen-Poiseuille equation assumes a circular cross section. To estimate the hydraulic impedance for noncircular cross sections, simply use Equation 2 where A is the cross-sectional area of the noncircular channel. The SI units for hydraulic impedance are Pa-s / m^3.

$$Z = \frac{\Delta P}{Q} = \frac{8\mu L}{\pi R^4} = \frac{8\pi\mu L}{A^2} \qquad \text{Eq. 2}$$

3. Propellant Degassing

Electrospray propulsion requires extended operation in a vacuum environment to be practical, which restricts the types of propellant that can be used. In particular, the propellant should have a low vapor pressure to minimize evaporative losses [26]. Further, volatile impurities can form gas bubbles in the Taylor cones or feed system, disrupting electrospray observation. We have observed gas bubbles emanating from Taylor cones (during electrospray emission) and from unperturbed liquid menisci (under no applied electric field), suggesting the presence of volatile impurities such as water in our ionic liquid propellants. These gas bubbles disrupted electrospray emission and tended to eject propellant in an uncontrolled manner, much of which impinged on the extractor grid and eventually led to backspray and an electrical short between the emitter array and the extractor.

Despite their low vapor pressures, many imidazolium-based ionic liquids are hydrophilic, making water removal difficult [27]. To remove volatile components from our propellant, the propellant reservoir was exposed to high vacuum (~10^{-5} Torr) for approximately 24 hours prior to each test. High vacuum was achieved by closing the N_2 and rough vacuum metering valves and opening the reservoir-to-chamber valve, providing a direct connection between the propellant vial and the high vacuum chamber. This procedure appeared to work well for Emi-Im, while the FAM-110A propellant proved more difficult to fully dry, possibly due to the hygroscopic nature of HAN [28]. For each propellant, this degassing procedure significantly improved electrospray emission stability and operational lifetime.

D. Diagnostics

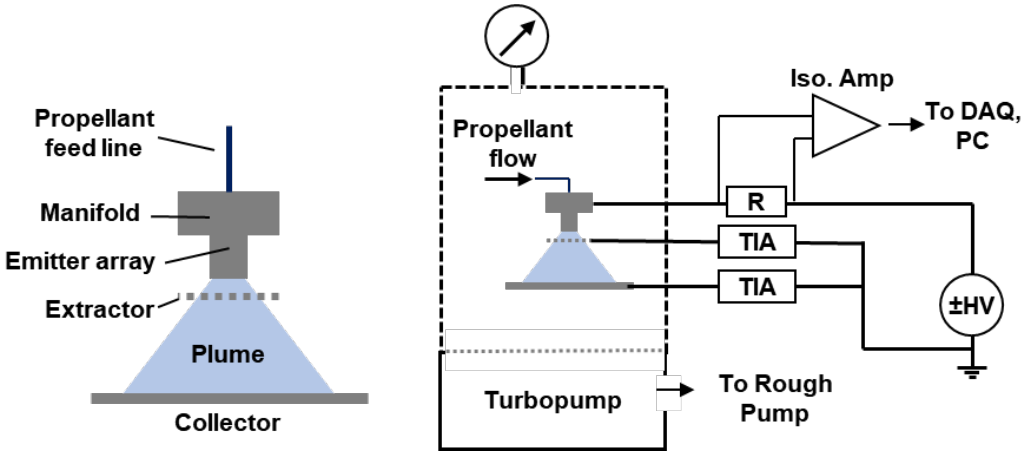

Figure 3: (Left) Diagram of thruster, plume, and current collector plate. (Right) Experimental overview showing vacuum chamber, thruster, and electrical connections. Propellant feed system not shown. Note: TIA = Transimpedance Amplifier, Iso. Amp = Isolation Amplifier, DAQ = Data Acquisition Device.

1. Emitter, Extractor, and Collector Current

Quantities measured during electrospray tests (Fig. 3) included the emitter and extractor currents, as well as the plume current measured by a 316 stainless steel collector plate. The collector plate intercepted the plume current up to an estimated 45° off centerline, intercepting >95% of the total plume current under typical operating conditions. Thus, by conservation of charge, the sum of the extractor and collector currents give an independent measurement of emitter current. Emitter current was measured using a current shunt and a high voltage isolation amplifier (Texas Instruments AMC1311) to remove the common mode voltage offset and interface with a data acquisition (DAQ) device (National Instruments USB-6210). Extractor and collector currents were conditioned using standard transimpedance amplifier configurations and recorded using the DAQ. Circuit protection against arcing or other overcurrent events was accomplished using Zener diodes with low leakage current ratings.

2. Retarding Potential Analyzer Measurements

Retarding potential analyzer (RPA) measurements were used to measure the kinetic energy profile of the electrospray plume, as is commonly done to characterize ion sources [29]–[32] . RPA data were collected by replacing the collector plate with a single grid RPA and Faraday cup (Kimball Physics FC-71). The FC-71 has a grounded front grid, and an electron suppression grid that was held at -30 V. The current measured by the Faraday cup was recorded as the retarding grid voltage was swept between ground and ±2.25 kV, with the polarity matching the emitter bias polarity. RPA data were analyzed by first applying a lowpass filter with a -3 dB cutoff frequency of 100 Hz. The data were then binned by retarding grid bias using a bin width of 25 V, and the median was calculated from the corresponding current measurements to yield the current value for that bin. Finally, the collector current was differentiated with respect to retarding grid bias to yield an intensity vs retarding bias plot that represents the energy profile of the electrospray plume.

3. Current-Voltage I-V Characteristic Curves

Current-voltage characteristic curves were collected by sweeping the emitter bias between -2.5 kV and +2.5 kV in 100 V increments using a 'stairstep' type waveform. This method was chosen to eliminate $d\varphi_{Emitter}/dt$ so that charging of the emitter capacitance did not interfere with emitter current measurements. Each stairstep lasted 10 ms. The first 5 ms of data are ignored while the emitter current stabilizes. Then, the median emitter current value is taken from the second 5 ms period as the current measurement.

IV. Results

A. Emi-Im

1. Long-duration test with Emi-Im

The MEPS thruster was first operated using the conventional electrospray propellant Emi-Im (also called Emi-Tf_2N) to demonstrate operability and to provide data for comparison to the literature. Figure 4 demonstrates over 10 hours of continuous electrospray emission using 6 active emitters. The emitter array was biased to 2,125 V with the polarity alternated at 0.5 Hz, while the extractor and collector were held at ground potential. The propellant feed pressure was 75.8 Torr, yielding an estimated total flow rate of 18.3 nL/s, or about 3 nL/s per emitter.

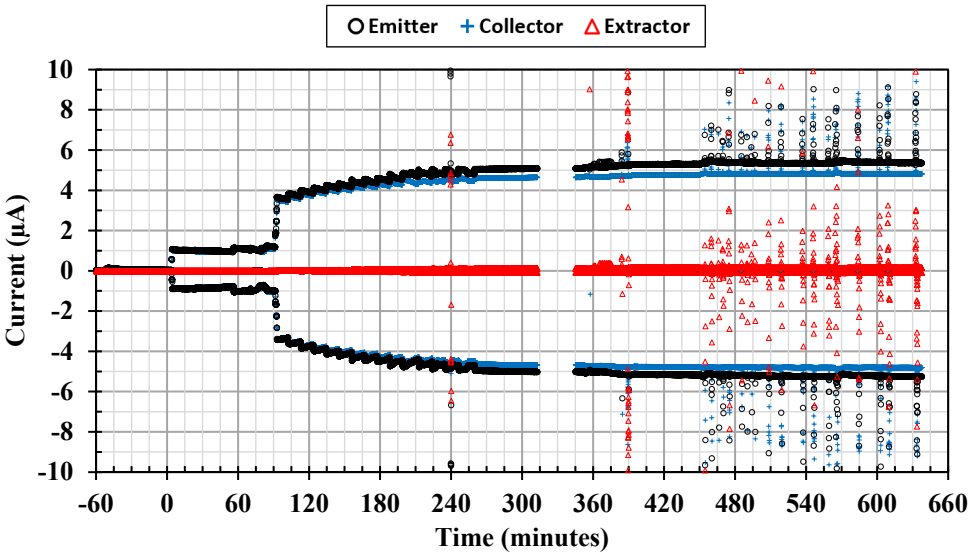

Figure 4: Electrospray-mode test of a 6-emitter test of the MEPS thruster with Emi-Im. The emitter array was biased to ±2,125 V with the extractor at ground. The propellant flow rate is estimated as 3 nL/s per emitter. Each data point represents a one-second average. Note the gap from t+310 min to t+330 min resulted from a data collection error, rather than malfunction of the thruster.

The startup transient of the thruster can be described as follows. At the start of a test, the emitter array is biased, and the propellant reservoir is backfilled to reach a specified feed pressure. Propellant begins to flow through the feed system, but dead volume causes a delay before the propellant reaches the thruster manifold. Once the manifold is

filled, propellant is forced into the thruster microchannels towards the emitter tips. Though the nominal dimensions of each channel is the same, manufacturing tolerances lead to variations in the hydraulic impedance. Thus, the channels fill at different rates. Propellant flows to the end of each channel, anchors at the emitter tip, forms a Taylor cone, and begins electrospray emission. Note that t=0 is synchronized with the first observation of electrospray emission. From t=0 to t+80 minutes, only some of the 6 open channels exhibit emission. At t+80 minutes, the increase in emission current indicates that all 6 open channels have begun emission. Between t+80 minutes and t+310 minutes, the emitter current slowly rises to steady state at about +5.4 μA (900 nA per emitter) for positive (cation) emission and -5.2 μA (870 nA per emitter) for negative (anion) emission. Some researchers using capillary emitters have measured negative emission currents 37% lower than positive emission currents at steady state for the same magnitude of applied voltage [5], while others report much closer symmetry between positive and negative emission [33]. Krpoun and Shea found that, for a single capillary emitter using Emi-Im, the negative emission current was approximately 2.4% lower in magnitude than the positive emission current [33]. Here, we have measured a negative emission current that is 3.7% lower than the positive emission current at steady state, well within the values reported in the literature.

As electrospray operation continues, the emitter and collector current measurements diverge, and the final values for collector current are +4.8 μA for positive emission and -4.8μA for anion emission. The cause of this divergence is not yet known, but several possible mechanisms have been identified. The simplest explanation is that the beam divergence increases with time, causing some of the plume to bypass the collector plate rather than impinge on it and produce a measurable current. The steady rise in extractor current from <5 nA at t+60 minutes to -90 nA and +145 nA at t+600 minutes for negative emission and positive emission, respectively, suggests that the beam divergence does indeed increase with time. Further, Figure 8 and the supporting discussion correlates a sudden rise in extractor impingement with a 'flooding' event in which excess propellant accumulates around the emitter tips. The slow accumulation of excess propellant around the emitter tips may explain the steady rise in beam divergence implied by rising extractor current, therefore we assess that increasing beam divergence is a plausible explanation for the difference between emitter and collector currents at late times.

Another possible explanation for the difference in emitter and collector currents is charge emission from surfaces due to ion bombardment. Ion induced charge emission has been studied for externally wetted, needle-type electrospray sources [34], [35]. There is evidence to suggest that both positive and negative species can be emitted from surfaces bombarded by ions in an electrospray beam, possibly due to the accumulation of a layer of ionic liquid on the collector surface [34]. Klosterman et al. studied charge emission due to ion bombardment from an Emi-BF_4 plume primarily consisting of monomers and dimers. They found that the negative charge yields from aluminum and molybdenum plates ranged from ~0.2 to ~1.2 for Emi-BF_4 ions with incident kinetic energies from 1.5 kV to 2.5 kV [35]. In contrast, xenon Xe^+ ions require kinetic energies of 7 kV to 14 kV to reach the same values for negative charge yield. These results suggest that electrospray ion bombardment may cause significantly higher secondary charge yields than traditional electric propulsion devices. Klosterman et al. also showed that target (collector) current varies considerably with target bias due to secondary charge emission effects. Biases of a few volts were shown to suppress charge emission from the target plate [35]. Due to the high secondary charge yield induced by electrospray ion bombardment and the apparent sensitivity of collector current to applied bias, we contend that secondary charge emission may play a role in accounting for the disparity in measured emitter and collector currents at late times in Figure 4. Measuring collector currents for different collector biases can help elucidate this role.

2. Retarding Potential Analysis of Emi-Im Plume

Retarding potential analyzer (RPA) measurements were collected for the MEPS thruster using Emi-Im to compare the plume energy distribution to single capillary emitter data in the literature. For this comparison, we define the energy deficit as the emitter potential minus the RPA potential, as in Equation 3. Thus, the energy deficit is the energy loss associated with extracting and accelerating ions and droplets.

$$\phi_{Deficit} = \phi_E - \phi_{RPA} \qquad \text{Eq. 3}$$

Figure 5 shows the energy deficit profile measured at the plume centerline of the MEPS thruster at ±2,125 V using Emi-Im at 3 nL/s per emitter. The energy deficit profile for a similarly sized capillary emitter [36] is plotted for comparison. This capillary emitter and the MEPS thruster are both low hydraulic impedance electrospray sources (>100 μm inner diameter), suggesting that they will operate in the mixed ion-droplet regime. Further, Gamero-Castaño used time-of-flight mass spectrometry to establish that the primary peak in the RPA data is due to ions, while the

wider 'tail' centered near 300 V is due to droplets [36]. Because the data match closely and the operating parameters (hydraulic impedance, extraction potential, etc.) are similar, here we assume that the MEPS data may be divided into two main peaks, the larger peak due to ions and the smaller peak due to droplets. Fitting the MEPS thruster data with a two-term gaussian, we find that the ion energy deficit is 550 V (FWHM = 118 V) and the droplet energy deficit is 294 V (FWHM = 648 V). Applying the same method to Gamero-Castaño's capillary emitter data, we find an ion energy deficit of 529 V (FWHM = 105 V) and a droplet energy deficit of 232 V (FWHM = 650 V).

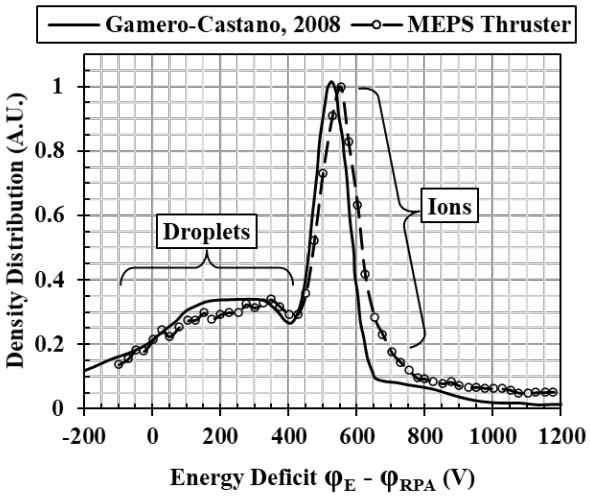

Figure 5: Energy deficit profile from this work and from a similarly sized capillary emitter [36]**. The primary peaks centered near 550 V and 529 V are attributed to ions. The broader, lower deficit peaks are attributed to droplets.**

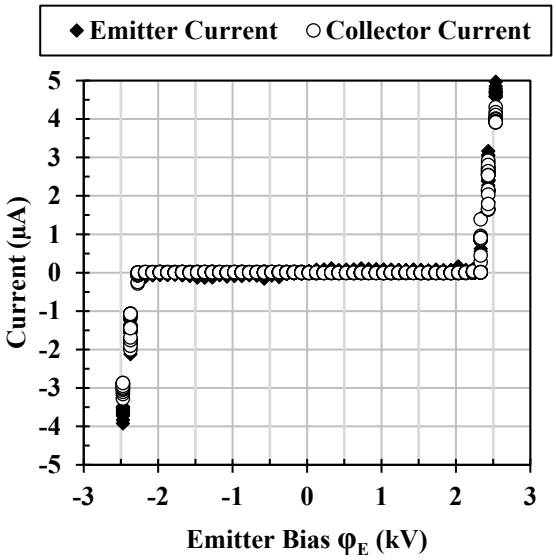

Figure 6: Emitter and collector currents as a function of emitter bias φ_E with four emitters active. Both polarities exhibit starting voltages of about 2.3 kV.

3. I-V Characteristic with Emi-Im

Another commonly used method of characterization for electrospray thrusters is the Current-Voltage (I-V) characteristic curve, as shown in Figure 6 for the MEPS thruster with 4 active emitters using Emi-Im. Figure 6 indicates that the starting voltage is roughly 2.3 kV for each polarity. Cation emission current reaches about +4.5 μA (1125 nA per emitter) at +2.5 kV emitter bias, while anion emission current reaches about -3.5 μA (-875 nA per emitter) at -2.5 kV emitter bias. These data were collected by sweeping emitter bias in 100 V steps with a step width of 10 ms. The emitter current is allowed to stabilize for 5ms, then the median current from the second 5 ms period is taken as the measured current for that emitter bias.

B. FAM-110A (59% HAN, 41% Emim-EtSO$_4$)

1. Long-duration test with FAM-110A

After demonstrating operability of the MEPS thruster with a conventional electrospray propellant (Emi-Im), efforts began to demonstrate extended operation of the thruster with the multimode-capable propellant FAM-110A. Figure 7 demonstrates continuous electrospray emission from 6 emitters of the MEPS thruster for over 4 hours using FAM-110A. Emitter bias was ±3,250 V, while the extractor and collector were held at ground potential. Propellant feed pressure was 102.9 Torr, yielding an estimated flow rate of 16.6 nL/s, or 2.77 nL/s per emitter. The startup transient lasts 60 minutes from first emission on one emitter to steady emission on 6 emitters. Emission current stabilizes at about +9.5 μA (+1580 nA per emitter) for cation mode, and about -8 μA (-1330 nA per emitter) for anion mode. Electrospray of FAM-110A from a single 100 μm capillary source at ±3.4 kV and ~3 nL/s produced emitter currents of +3194 nA and -2011 nA in positive and negative emission mode, respectively [5]. The per-emitter current is lower for the MEPS thruster than for the single emitter, but the asymmetry between positive and negative emission currents is less severe (37% vs 3.7%). It is possible that electrostatic shielding reduces the electric field strength for the multi-emitter thruster, thus extracting a lower beam current.

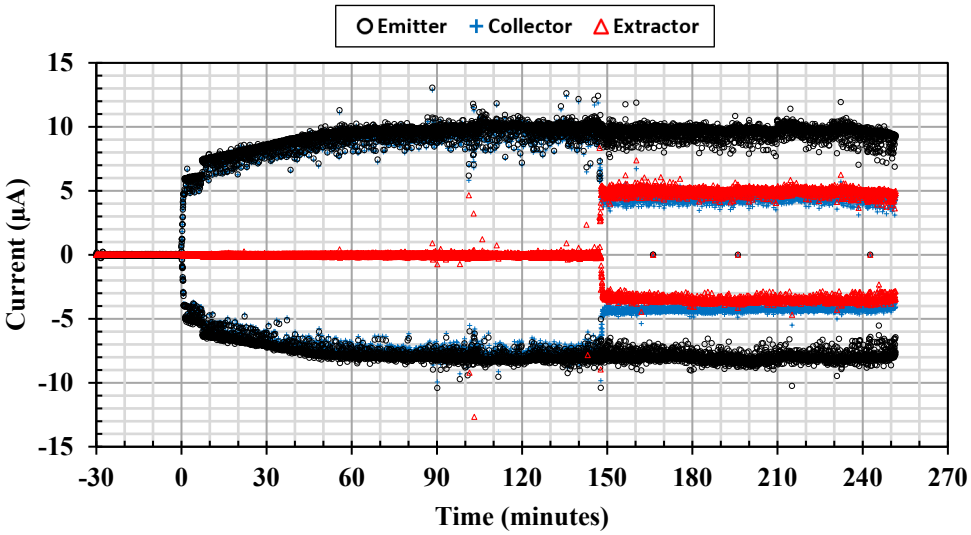

Figure 7: Electrospray-mode test of a 6-emitter subset of the MEPS thruster with multimode propellant FAM-110A. The emitter array was biased to ±3,250 V with the extractor at ground. The propellant flow rate is estimated as 2.77 nL/s per emitter.

The most striking feature of the FAM-110A data is the step change in extractor impingement around t+148 minutes. From t=0 to t+148 minutes, extractor impingement increases from 1.3% to 2.3% of the total emitter current. At t+148 minutes, extractor impingement increases from 2.3% to 42% of the emitter current over 30 seconds. Although no video is available from t+148 minutes, we have observed similar rises in impingement current for Emi-Im. Figure 8 shows video stills taken during an electrospray test with Emi-Im, showing the array block, emitter tips, and extractor electrode in profile. Figure 8A shows the conditions when the first electrospray emission was detected, and only one emitter was spraying. For ~90 minutes the extractor current stayed nearly constant at 0.2% of the emitter current, then rose to 1.0% over 15 minutes (Figure 8B). The extractor current then rapidly increased from 1.0% to 48.2% of the emitter current over only 15 seconds. Figure 8C shows the thruster operating with 48.2% extractor impingement less than a minute after Figure 8B.

The apparent cause of the drastic increase in impingement fraction is a 'flooding' event, in which excess propellant surrounds the emitter tips and interferes with electrospray emission. The most feasible explanation for the rise in extractor impingement is that the flooding event caused the electrospray plume to broaden, though it is not immediately clear how this would occur. One possible explanation is that the electric field concentration and shaping provided by the emitter tips is modified when the conductive propellant surrounds the tips and reduces their effective height. Whatever the cause, flooding of the emitter tips is a common issue with capillary thrusters that may end their operational life. Consequently, flooding should be mitigated wherever possible through careful thruster and feed system design, and by thoroughly degassing propellant before use.

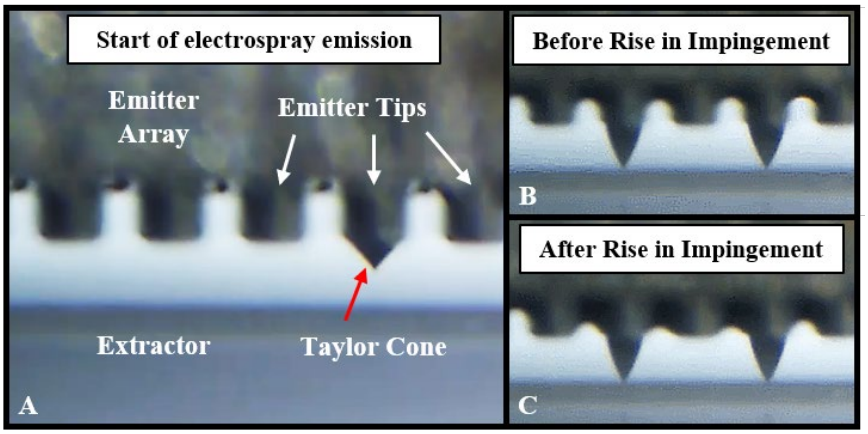

Figure 8: View of the MEPS microthruster emitter tips in profile. (A) Propellant flows through the emitter array to the emitter tips, where it forms a Taylor cone and emits a beam of ions and charged droplets. Propellant tends to accumulate on around the emitter tips during extended operation. (B) and (C) show the conditions before and after a sudden rise in extractor impingement, respectively. These images show that excess propellant 'flooding' the emitter tips is responsible for the high extractor impingement fraction.

V. Discussion

1. Lifetime-Limiting Mechanisms: Backspray and Flooding

Capillary electrospray thrusters have generally exhibited short lifetimes compared to mature electric propulsion technologies [37]. Several failure mechanisms have been investigated, including electron backstreaming [38], electrochemical degradation of the propellant [39], [40], and overspray leading to extractor or accelerator grid saturation [37], [41]–[43]. Here we examine backspray, which is regarded as the primary life-limiting mechanism for capillary electrospray thrusters [37], [41]. We also discuss accumulation of propellant around the emitter tips, which we call 'flooding'. These two mechanisms account for most of the end-of-test conditions for MEPS thruster tests to date. We find that minor adjustments to the emitter-extractor distance and alignment can significantly delay the onset of backspray, while flooding is best prevented by careful feed system design and thorough degassing of the propellant.

Extractor impingement, also called grid impingement or overspray, is the unintentional deposition of propellant on the extractor and/or accelerator electrodes that results from the wide angle of the electrospray plume. Non-negligible mass fluxes have been measured in electrospray plumes as far as 50° off axis [44], and any mass flux in the plume must either pass through the extractor aperture or impinge on the extractor grid. Some researchers have used porous grids to absorb propellant that impinges on the grids and delay backspray [37], but a reduction of the impinging mass flux is a more desirable solution.

Here, we have observed extractor impingement fractions as low as 0.2% of the total emitter current for ~90 minutes. The test conditions were Emi-Im spraying from six emitters at a feed rate of ~3 nL/s per emitter and an emitter potential of ±2,125 V with the polarity alternated at 0.5 Hz. The emitter-extractor gap was 500 µm and the extractor aperture was a ~1250 µm wide slot, yielding a half-angle of acceptance of ~50° as measured from the emitter tip. That is, we estimate that mass flux in the plume that is <50° off centerline will pass through the extractor aperture, and mass flux >50° off centerline will impinge on the extractor grid. Figure 9 shows the MEPS microthruster in profile, with three emitters spraying downward toward the extractor grid. A Taylor cone can also be seen on the extractor grid, backspraying propellant towards the emitter tips. This backspray can lead to flooding of the emitter tips, electrical arcing, and/or chemical degradation of propellant due to high-energy ion bombardment. We have observed considerable sensitivity to misalignment, though it was not well quantified.

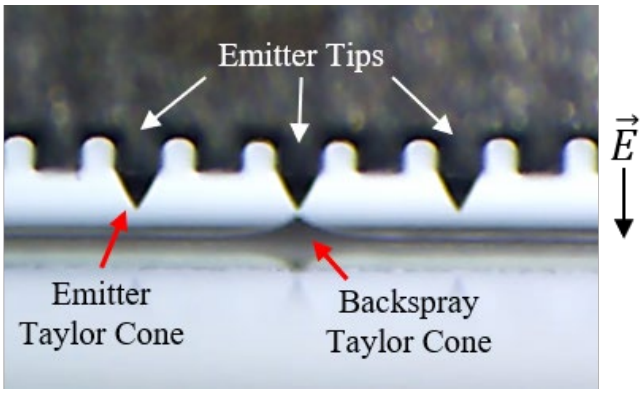

Figure 9: 'Backspray' due to ionic liquid (IL) propellant accumulation on the extractor grid. If extractor impingement is high, e.g. due to improper extractor alignment, IL will collect on the extractor. When enough IL has collected, it will form a Taylor cone on the extractor that sprays back towards the emitter array.

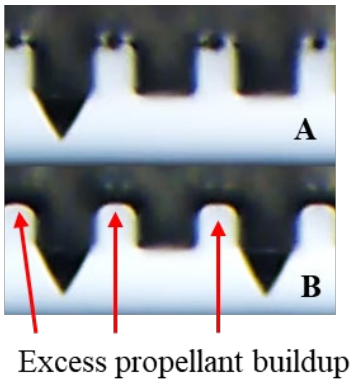

Figure 10: 'Flooding' of the emitter tips sometimes occurs during long tests. (A) The tips are clean at the start of electrospray emission, and (B) the tips are partially flooded after several hours of electrospray operation.

The second life-limiting mechanism that we observed during testing is flooding of the emitter tips with excess propellant. Flooding has many causes, including transient instabilities at thruster startup, excessively high flow rate, and film wicking along wetting surfaces. Thruster startup transients can be reduced by closely matching the hydraulic impedance of the microchannel emitters so that they begin electrospray emission around the same time, and so the flow rate is consistent across emitters in the array. We found that the longest test durations were achieved by using the lowest flow rate that could sustain continuous electrospray emission. Low propellant flow rates tend to reduce droplet emission, presumably reducing grid impingement. Low flow rates also reduce the risk of overflowing any of the emitter tips, which occurs when the sum of the feed pressure and electrostatic pressure are much higher than the surface tension pressure at the emitter tip. This excess pressure can lead to a flow rate through the affected emitter that is too high to be matched by propellant removal via electrospray emission, causing an overflow of the emitter tip.

Another potential cause of flooding is propellant wicking across wetting surfaces. The topic of wetting is well-studied in electrospray [45]–[48], though it remains a persistent challenge. Surface wettability is, in general, a function of the surface material and roughness as well as the liquid properties. Researchers have attempted to reduce surface wettability of the emitters by using hydrophobic materials, such as polymers [48], [49], and have successfully enhanced wetting by surface treatments such as with black-silicon [48], [50], [51]. Our goal is to characterize the MEPS thruster as is, so we do not explore surface treatments to modify wettability in this work.

We also observed the uncontrolled ejection of propellant from the capillary microchannels due to the presence of volatiles in the propellant, which sometimes led to flooding and/or grid impingement. We found that thoroughly degassing the propellant at high vacuum ($< 10^{-5}$ Torr) for 24 hours was effective at reducing the water content of Emi-Im enough to suppress gas bubble formation in the capillary microchannels or Taylor cones. FAM-110A is synthesized with <1% water content, but it is more hygroscopic than Emi-Im due to its HAN content. We found that the most effective route to keeping the moisture content of FAM-110A low was to minimize its exposure to humidity after its synthesis.

2. Effect of Hydraulic Impedance on Operating Regime

It is well established that pure ion emission can be achieved with capillary emitters only at low flow rates and with highly conductive propellants, if at all [26]. Less well understood is the relationship between the minimum flow rate for stable electrospray emission and the inner diameter of the capillary emitter. A related quantity, known as the hydraulic impedance or hydraulic resistance (Equation 2), describes the resistance of a capillary to fluid flow. Several authors have described the role of hydraulic impedance in determining the performance of capillary electrospray devices [33], [51]–[54]. For example, Krpoun et al. tested a capillary thruster with 24 µm capillary channels both with and without added silica microbeads for increased hydraulic impedance [52]. They showed that increasing the hydraulic impedance of the channels resulted in a shift toward pure ion emission and a reduction in ion energy deficit. The role of hydraulic impedance in determining capillary thruster performance has not been thoroughly quantified, making the design of capillary electrospray devices challenging.

Figure 11 compares the hydraulic impedance of capillary-type thrusters from the literature. The thrusters with higher hydraulic impedance ($>10^{16}$ Pa-s/m^3) tend towards pure ion emission, while thrusters with a lower hydraulic impedance operate in the mixed ion-droplet regime. Note that Dandavino et al. use Emi-BF_4 as a propellant, Lenguito et al. use ethyl ammonium nitrate (EAN), and Alexander et al. use Bmim-BF_4, while Krpoun et al. and this work (MEPS thruster) use Emi-Im. Pure ion emission generally results in greater thruster efficiency and higher specific impulse than mixed ion-droplet emission, but with a lower thrust to power ratio.

In addition to hydraulic impedance, we can consider the tendency of propellant to overflow the emitter tips and flood the thruster with excess propellant, which often results in an electrical short and end-of-life for the thruster. For this, we consider the surface tension pressure, which refers to the pressure jump across the liquid-vacuum interface when no electric field is applied to the emitter tip. This pressure jump is a consequence of surface tension, and scales with 1/R where R is the radius of the liquid meniscus. Surface tension pressure can also be interpreted as the maximum feed pressure that may be applied (with no applied electric field) before propellant overflows the emitter tip and floods the surrounding area with excess propellant. As such, it can be used to quantify how easily a capillary electrospray device can be flooded by excessive propellant feed pressure.

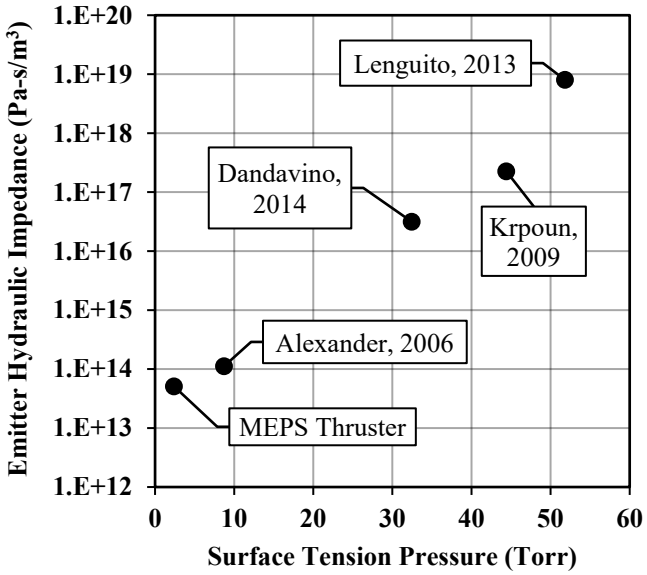

Figure 11: Comparison of capillary electrospray thrusters. Dandavino, Lenguito, and Krpoun observed pure ion emission from their thrusters [25], [33], [53]**, while mixed ion-droplet emission was seen in this work and by Alexander** [55]**. High hydraulic impedance emitters can maintain a stable electrospray at lower flow rates than their larger counterparts, allowing them to suppress droplet emission. Hydraulic impedances were calculated using Equation 2.**

The concept of surface tension pressure can aid in the design of capillary electrospray devices. For example, Velásquez-García used this concept in the design of a internally-fed thruster that implements electrical control of flow rate and electrospray emission [51]. A feed pressure is applied that is smaller than the surface tension pressure, thus no propellant flows. A voltage difference is then applied between the emitters and the extractor electrode, creating an electrostatic pressure on the liquid meniscus. The sum of the electrostatic pressure and the feed pressure is larger than the surface tension pressure, thus allowing propellant to flow and feed the electrospray emission. When the applied voltage is removed, flow stops again. Thus, surface tension has been used to implement electrical control of a capillary thruster.

3. Effect of Beam Current on Ion Energy Deficit

Ion energy deficit has been measured for various electrospray sources, both internally and externally wetted. Lozano measured ion energy deficits for an externally wetted needle emitter using Emi-Im [31]. He found ion energy deficits of 5±1 eV to 7±1 eV over a range of emitter biases, with FWHM around 6 eV to 8 eV. Lozano concludes that the energy deficits he measured are primarily due to the energy required to evaporate ions from the liquid propellant into the gas phase. Further, he confirms that no droplets are present in the plume using time-of-flight mass

spectrometry. Together, these data suggest that his externally wetted electrospray source emits ions by field evaporation from the Taylor cone, rather than from a cone-jet structure emanating from the emitter.

In stark contrast, Gamero-Castaño's experiments using Emi-Im showed ion energy deficits of 200-700 eV from a 160 μm capillary emitter operating in the mixed ion-droplet regime [36]. In this regime, a narrow jet emanates from the tip of the Taylor cone, gaining kinetic energy in exchange for electrical potential energy as it travels towards the extractor. Within the acceleration region, instabilities cause the jet to break up into a spray of charged droplets. Ion extraction can occur anywhere along the liquid-vacuum interface where the electric field normal to the surface is sufficiently high for field evaporation, generally believed to be around 1 V/nm [31]. Gamero-Castaño notes that the large disparity in mass to charge ratio between ions and droplets results in the ion energy being nearly identical to the electrical potential at the point of their extraction from the liquid phase. He identified two populations of particles in his electrospray plume, ions and droplets, and saw that the energy deficit for ions was higher than the deficit for droplets. Further, the ion energy deficit increased with higher emitter currents and flow rates. He proposed that ions were being emitted from the jet breakup region, and that higher beam currents and flow rates delay jet breakup. This causes breakup to occur further into the extraction region at a lower potential, thereby increasing the ion energy deficit.

Figure 12 shows the effect of emitter current on ion energy deficit for three capillary-type electrospray sources using Emi-Im. In addition to Gamero-Castaño's data, three data sets from this work are plotted, as well as Krpoun's data for a high hydraulic impedance capillary thruster operating in the pure ion regime [33]. Our data closely match Gamero-Castaño's data over the range measured in our experiments, showing a similar trend. Notably, our data were collected at an estimated propellant flow rate of 3 nL/s per emitter while Gamero-Castaño used a flow rate of about 1.1 nL/s for his 573 nA data point. Despite this significant different in flow rates, the beam currents are similar as is the resulting ion energy deficit. These data suggest that emitter current may be a better predictor of jet breakup than propellant flow rate, potentially due to space charge effects.

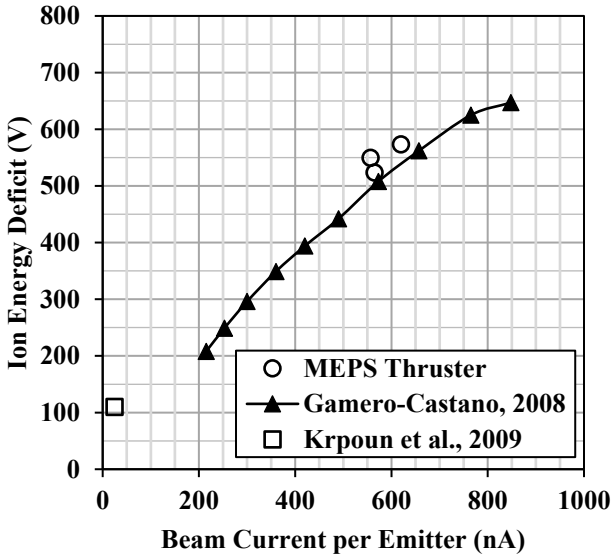

Figure 12: Ion energy deficit as a function of emitter current. Ions emitted in the mixed ion-droplet mode have a larger energy deficit than those emitted in pure ion emission mode (e.g., Krpoun et al. [33]**).**

Figure 13 shows the energy deficit profiles for the low hydraulic impedance thruster used in this work and the high hydraulic impedance thruster studied by Krpoun [33]. The first observation is that the large peak, which is due to ions, occurs at a much lower energy deficit for the high hydraulic impedance thruster, implying more efficient operation. Considering the low hydraulic impedance data, the large 'tail' to the left of the peak is the contribution of droplets. No such 'tail' is seen in the high hydraulic impedance thruster data, implying operation in or near the pure ion regime. Krpoun notes that their data were collected using a single grid RPA, which is known to be less accurate than multi-grid RPAs [29]–[31], [33]. Krpoun estimates that the true ion energy deficit may be less than 50 V.

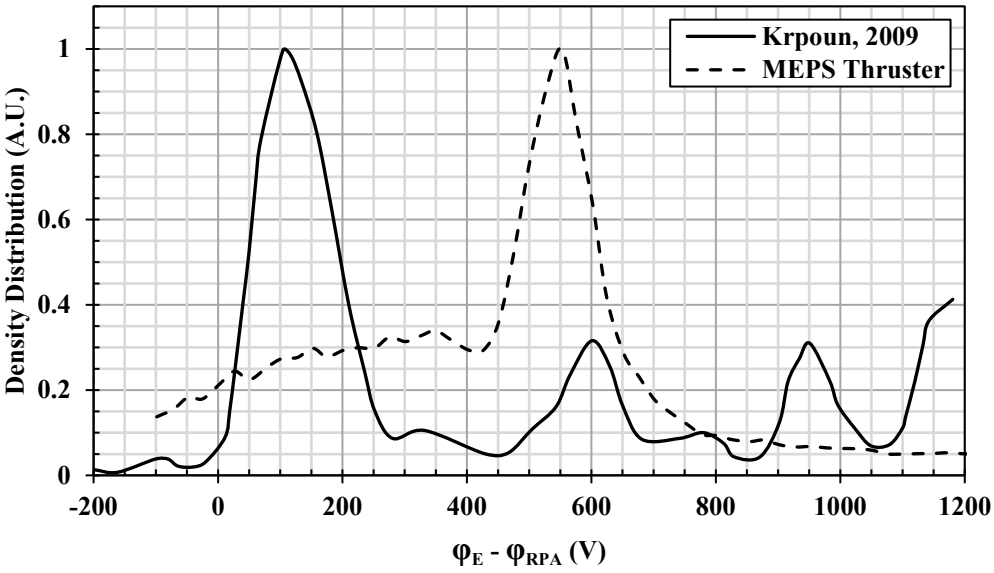

Figure 13: Energy deficit profile for two capillary electrospray thrusters using Emi-Im. This work (dashed line) uses 6 active emitters, each with an area-equivalent diameter of about 140 µm. Krpoun (solid line) uses a 19-emitter array, each with an inner diameter of 24 µm [33]**. Krpoun further increases hydraulic impedance by filling the emitter capillaries with silica microspheres.**

VI. Conclusion

We have demonstrated for the first time that a propellant specifically designed for multimode monopropellant-electrospray propulsion, FAM-110A (59% wt. HAN, 41% wt. [Emim][$EtSO_4$], <1% wt. H_2O), can be stably electrosprayed from a multi-emitter capillary thruster. Further, we demonstrated for the first time the stable electrospray operation of a novel multimode thruster capable of switching between monopropellant and electrospray modes. We operated a six-emitter subset of the thruster using the multimode propellant FAM-110A for more than four hours, and for more than ten hours using the conventional electrospray propellant Emi-Im. As with other capillary electrospray thrusters, the most common end-of-test condition was buildup of excess propellant either (1) on and around the emitter tips, leading to flooding, or (2) on the extractor electrode, eventually leading to backspray and electrical arcing.

Retarding potential measurements of an Emi-Im plume from the thruster indicate an ion energy deficit of about 550 V (FWHM = 118 V). Comparison to similarly sized single capillary emitters in the literature shows a nearly identical plume energy profile, indicating that there is a mixture of ions and charged droplets in the thruster plume. The previously observed trend of ion energy deficit increasing with beam current (or propellant flow rate) is also observed here. Our data were taken at higher flow rates, but similar beam currents (per emitter) compared with the single emitter work of Gamero-Castaño, suggesting that the jet breakup dynamics are more sensitive to beam current than flow rate. Although not measured here, the specific impulse could likely be improved by moving to lower propellant flow rates, which may require higher hydraulic impedance microchannels (emitters) to maintain a stable electrospray emission.

Hydraulic impedance, or the resistance to fluid flow, has been briefly discussed in the context of capillary electrospray sources. It is well established that pure ion emission is possible at low propellant flow rates, while higher flow rates produce a mix of ions and droplets. However, flow rate cannot be arbitrarily decreased while maintaining electrospray stability. The minimum stable flow rate appears to be related to the emitter hydraulic impedance, although this author has not seen a quantitative analysis of that relationship. A quick review of capillary-type electrospray thrusters in the literature suggests that an emitter hydraulic impedance greater than 10^{16} Pa-s/m^3 favors ion emission, while a hydraulic impedance lower than 10^{14} Pa-s/m^3 produces droplet-heavy electrospray emission. Large droplet fractions are known to decrease specific impulse and efficiency but increase the thrust to power ratio compared to pure ion emission. Further investigation is needed to understand and quantify the effects of hydraulic impedance on the minimum flow rate for stable electrospray emission, especially in the context of multi-emitter capillary thrusters.

VII. Acknowledgements

This work was partially supported by a NASA Space Technology Research Fellowship for Chris Lyne, NASA Grant 80NSSC19K1165, with technical monitor Chris Burnside and by a NASA SBIR Phase II program grant to Froberg Aerospace LLC, NASA contract number 80NSSC18C0074, with technical monitor Dr. John Yim. We would also like to thank Dr. Ben Prince and Dr. Shawn Miller for their help in understanding capillary electrospray troubleshooting and time-of-flight mass spectroscopy.

VIII. References

[1] B. Doncaster, J. Shulman, J. Bradford, and J. Olds, "SpaceWorks' 2016 Nano/Microsatellite Market Forcast," *Proc. AIAA/USU Conf. Small Satell. Mission Lessons, SSC16-II-01*, pp. 1–6, 2016.

[2] D. Krejci and P. Lozano, "Space Propulsion Technology for Small Spacecraft," *Proc. IEEE*, vol. 106, no. 3, pp. 362–378, 2018.

[3] S. P. Berg and J. L. Rovey, "Assessment of Multimode Spacecraft Micropropulsion Systems," *J. Spacecr. Rockets*, vol. 54, no. 3, pp. 592–601, 2017.

[4] J. L. Rovey *et al.*, "Review of multimode space propulsion," *Prog. Aerosp. Sci.*, vol. 118, p. 100627, 2020.

[5] S. P. Berg, J. Rovey, B. Prince, S. Miller, and R. Bemish, "Electrospray of an Energetic Ionic Liquid Monopropellant for Multi-Mode Micropropulsion Applications," in *51st AIAA/SAE/ASEE Joint Propulsion Conference*, American Institute of Aeronautics and Astronautics, 2015.

[6] S. P. Berg and J. L. Rovey, "Assessment of Imidazole-Based Ionic Liquids as Dual-Mode Spacecraft Propellants," *J. Propuls. Power*, vol. 29, no. 2, pp. 339–351, 2013.

[7] B. R. Donius and J. L. Rovey, "Ionic Liquid Dual-Mode Spacecraft Propulsion Assessment," *J. Spacecr. Rockets*, vol. 48, no. 1, pp. 110–123, 2011.

[8] E. Fonda-Marsland and C. Ryan, "Preliminary Ionic Liquid Propellant Selection for Dual-Mode Micro-Propulsion Systems," in *53rd AIAA/SAE/ASEE Joint Propulsion Conference*, 2017.

[9] S. P. Berg and J. L. Rovey, "Dual-Mode Propellant Properties and Performance Analysis of Energetic Ionic Liquids," *50th AIAA Aerosp. Sci. Meet.*, no. January, p. AIAA 2012-0975, 2012.

[10] S. Berg and J. Rovey, "Ignition Evaluation of Monopropellant Blends of HAN and Imidazole-Based Ionic Liquid Fuels," *50th AIAA Aerosp. Sci. Meet. Incl. New Horizons Forum Aerosp. Expo.*, no. January, p. AIAA-2012-0974, 2012.

[11] S. P. Berg and J. L. Rovey, "Decomposition of Monopropellant Blends of Hydroxylammonium Nitrate and Imidazole-Based Ionic Liquid Fuels," *J. Propuls. Power*, vol. 29, no. 1, pp. 125–135, 2013.

[12] A. Mundahl, S. P. Berg, and J. Rovey, "Linear Burn Rates of Monopropellants for Multi-Mode Micropropulsion," *52nd AIAA/SAE/ASEE Jt. Propuls. Conf.*, pp. 1–11, 2016.

[13] S. P. Berg and J. Rovey, "Decomposition of a Double Salt Ionic Liquid Monopropellant in a Microtube for Multi-Mode Micropropulsion Applications," in *53rd AIAA/SAE/ASEE Joint Propulsion Conference*, American Institute of Aeronautics and Astronautics, 2017.

[14] A. J. Mundahl *et al.*, "Characterization of a novel ionic liquid monopropellant for multi-mode propulsion," in *53rd AIAA/SAE/ASEE Joint Propulsion Conference*, 2017, p. 4756.

[15] A. J. Mundahl, J. Rovey, and S. P. Berg, "Linear Burn Rate of Monopropellant for Multi-Mode Micropropulsion," in *AIAA-2018-2018-4970, 2018 Joint Propulsion Conference*, 2018.

[16] N. Rasmont, E. J. Broemmelsiek, and J. L. Rovey, "Linear burn rate of green ionic liquid multimode monopropellant," *Combust. Flame*, vol. 219, pp. 212–224, 2020.

[17] M. J. Wainwright, S. Miller, B. D. Prince, S. P. Berg, and J. Rovey, "Mass Spectroscopy of a Multi-Mode Propellant in Anion and Cation Mode," in *2018 Joint Propulsion Conference*, 2018.

[18] M. J. Wainwright, J. L. Rovey, S. W. Miller, B. D. Prince, and S. P. Berg, "Hydroxylammonium nitrate species in a monopropellant electrospray plume," *J. Propuls. Power*, vol. 35, no. 5, pp. 922–929, 2019.

[19] S. P. Berg, M. S. Glascock, M. Cooper, and J. L. Rovey, "Multimode Integrated Monopropellant Electrospray Thruster Testing Results: Chemical Mode," in *NASA In-Space Chemical Propulsion Technical Interchange Meeting*, 2020.

[20] D. Zube, S. Christofferson, E. Wucherer, and B. Reed, "Evaluation of HAN-Based Propellant Blends," in *39th AIAA/ASME/SAE/ASEE Joint Propulsion Conference and Exhibit*, 2003, no. July.

[21] J. A. Boatz, G. A. Voth, M. S. Gordon, and S. Hammes-Schiffer, "Design of Energetic Ionic Liquids," in *2010 DoD High Performance Computing Modernization Program Users Group Conference*, 2010, pp. 201–207.

[22] D. Amariei *et al.*, "Influence of Fuel on Thermal and Catalytic Decompositions of Ionic Liquid Monopropellants," in *41st AIAA/ASME/SAE/ASEE Joint Propulsion Conference and Exhibit*, 2005, no. July,

pp. 1–9.
[23] H. Meng, P. Khare, G. Risha, R. Yetter, and V. Yang, "Decomposition and Ignition of HAN-Based Monopropellants by Electrolysis," in *47th AIAA Aerospace Sciences Meeting*, 2009, no. January, pp. 1–17.
[24] Y.-P. Chang and K. Kuo, "Assessment of combustion characteristics and mechanism of a HAN-based liquid monopropellant," in *37th Joint Propulsion Conference and Exhibit*, 2001, no. July.
[25] S. Dandavino *et al.*, "Microfabricated electrospray emitter arrays with integrated extractor and accelerator electrodes for the propulsion of small spacecraft," *J. Micromechanics Microengineering*, vol. 24, no. 7, 2014.
[26] P. C. Lozano, "Studies on the ion-droplet mixed regime in colloid thrusters," PhD dissertation, MIT, Department of Aeronautics and Astronautics, 2003. 29, 2003.
[27] T. Takamuku, Y. Kyoshoin, T. Shimomura, S. Kittaka, and T. Yamaguchi, "Effect of water on structure of hydrophilic imidazolium-based ionic liquid," *J. Phys. Chem. B*, vol. 113, no. 31, pp. 10817–10824, 2009.
[28] H. Lee and T. A. Litzinger, "Thermal decomposition of han-based liquid propellants," *Combust. Flame*, vol. 127, no. 4, pp. 2205–2222, Dec. 2001.
[29] C. L. Enloe, "High-resolution retarding potential analyzer," *Rev. Sci. Instrum.*, vol. 65, no. 2, pp. 507–508, 1994.
[30] C. L. Enloe and J. R. Shell, "Optimizing the energy resolution of planar retarding potential analyzers," *Rev. Sci. Instrum.*, vol. 63, no. 2, pp. 1788–1791, 1992.
[31] P. C. Lozano, "Energy properties of an EMI-Im ionic liquid ion source," *J. Phys. D. Appl. Phys.*, vol. 39, no. 1, pp. 126–134, 2006.
[32] S. W. Miller, B. D. Prince, R. J. Bemish, and J. L. Rovey, "Electrospray of 1-Butyl-3-Methylimidazolium Dicyanamide Under Variable Flow Rate Operations," *J. Propuls. Power*, vol. 30, no. 6, pp. 1701–1710, 2014.
[33] R. Krpoun and H. R. Shea, "Integrated out-of-plane nanoelectrospray thruster arrays for spacecraft propulsion," *J. Micromechanics Microengineering*, vol. 19, no. 4, 2009.
[34] M. R. Klosterman, "Ion-induced Charge Emission from Surfaces Bombarded by an [Emim][BF4] Electrospray Plume," University of Illinois Urbana-Champaign, 2021.
[35] M. R. Klosterman, J. L. Rovey, and D. A. Levin, "Ion-induced Charge Emission from Surfaces Bombarded by an [Emim][BF4] Electrospray Plume," *J. Appl. Phys. – Spec. Issue Phys. Electr. Propulsion, Rev.*
[36] M. Gamero-Castaño, "Characterization of the electrosprays of 1-ethyl-3-methylimidazolium bis(trifluoromethylsulfonyl) imide in vacuum," *Phys. Fluids*, vol. 20, no. 3, 2008.
[37] A. Thuppul, P. L. Wright, A. L. Collins, J. K. Ziemer, and R. E. Wirz, "Lifetime Considerations for Electrospray Thrusters," *Aerospace*, vol. 7, no. 8. 2020.
[38] K. J. Terhune, L. B. King, K. He, and J. Cumings, "Radiation-induced solidification of ionic liquid under extreme electric field," *Nanotechnology*, vol. 27, no. 37, p. 375701, 2016.
[39] N. Brikner and P. C. Lozano, "The role of upstream distal electrodes in mitigating electrochemical degradation of ionic liquid ion sources," *Appl. Phys. Lett.*, vol. 101, no. 19, p. 193504, Nov. 2012.
[40] P. Lozano and M. Martínez-Sánchez, "Ionic liquid ion sources: Suppression of electrochemical reactions using voltage alternation," *J. Colloid Interface Sci.*, vol. 280, no. 1, pp. 149–154, 2004.
[41] P. N. Dahl, A. M. Kimber, and B. A. Jorns, "Data-driven scaling law for the extractor current of a capillary electrospray," *AIAA Propuls. Energy Forum Expo. 2019*, no. August, pp. 1–10, 2019.
[42] R. E. Wirz *et al.*, "Electrospray thruster performance and lifetime investigation for the LISA mission," *AIAA Propuls. Energy Forum Expo. 2019*, no. August, 2019.
[43] P. L. Wright, A. Thuppul, and R. E. Wirz, "Life-limiting emission modes for electrospray thrusters," *2018 Jt. Propuls. Conf.*, pp. 1–9, 2018.
[44] S. W. Miller, B. D. Prince, R. J. Bemish, and J. L. Rovey, "Electrospray of 1-butyl-3-methylimidazolium dicyanamide under variable flow rate operations," *J. Propuls. Power*, vol. 30, no. 6, pp. 1701–1710, 2014.
[45] Q. Xue, F. Foret, Y. M. Dunayevskiy, P. M. Zavracky, N. E. McGruer, and B. L. Karger, "Multichannel microchip electrospray mass spectrometry," *Anal. Chem.*, vol. 69, no. 3, pp. 426–430, 1997.
[46] B. Zhang, H. Liu, B. L. Karger, and F. Foret, "Microfabricated devices for capillary electrophoresis-electrospray mass spectrometry," *Anal. Chem.*, vol. 71, no. 15, pp. 3258–3264, 1999.
[47] P. Lozano, M. Martínez-Sánchez, and J. M. Lopez-Urdiales, "Electrospray emission from nonwetting flat dielectric surfaces," *J. Colloid Interface Sci.*, vol. 276, no. 2, pp. 392–399, 2004.
[48] L. F. Velásquez-García, A. I. Akinwande, and M. Martínez-Sánchez, "A planar array of micro-fabricated electrospray emitters for thruster applications," *J. Microelectromechanical Syst.*, vol. 15, no. 5, pp. 1272–1280, 2006.
[49] M. S. Lhernould and P. Lambert, "Compact polymer multi-nozzles electrospray device with integrated microfluidic feeding system," *J. Electrostat.*, vol. 69, no. 4, pp. 313–319, 2011.

[50] B. Gassend, L. F. Velasquez-Garcia, A. I. Akinwande, and M. Martinez-Sanchez, "A Microfabricated Planar Electrospray Array Ionic Liquid Ion Source With Integrated Extractor," *J. Microelectromechanical Syst.*, vol. 18, no. 3, pp. 679–694, 2009.
[51] L. F. Velásquez-garcía, A. I. Akinwande, and M. Martínez-sánchez, "A Micro-Fabricated Linear Array of Electrospray Emitters for Thruster Applications," vol. 15, no. 5, pp. 1260–1271, 2006.
[52] R. Krpoun, K. L. Smith, J. P. W. Stark, and H. R. Shea, "Tailoring the hydraulic impedance of out-of-plane micromachined electrospray sources with integrated electrodes," *Appl. Phys. Lett.*, vol. 94, no. 16, 2009.
[53] G. Lenguito and A. Gomez, "Development of a multiplexed electrospray micro-thruster with post-acceleration and beam containment," *J. Appl. Phys.*, vol. 114, no. 15, pp. 1–8, 2013.
[54] E. Grustan-Gutierrez and M. Gamero-Castaño, "Microfabricated electrospray thruster array with high hydraulic resistance channels," *J. Propuls. Power*, vol. 33, no. 4, pp. 984–991, 2017.
[55] M. S. Alexander, J. Stark, K. L. Smith, B. Stevens, and B. Kent, "Electrospray performance of microfabricated colloid thruster arrays," *J. Propuls. Power*, vol. 22, no. 3, pp. 620–627, 2006.